Neuro-Mimetic Dynamics of a Ferroelectric FET-Based Spiking Neuron

Yan Fang, *Member, IEEE*, Jorge Gomez, *Student Member, IEEE*, Zheng Wang, *Student Member, IEEE*, Suman Datta, *Fellow, IEEE*, Asif I. Khan, *Member, IEEE*, and Arijit Raychowdhury, *Senior Member, IEEE*

***Abstract*— We demonstrate that a ferroelectric field-effect transistor (FeFET)-based spiking neuron is capable of mimicking various spiking and bursting patterns characteristic of cortical neurons. We propose a compact model to describe the dynamical behavior of such FeFET-based spiking neurons. This model captures the current-voltage dynamics of the FeFET and the critical voltages of its hysteretic region. It is aimed at system-level modeling and simulation of biomimetic networks of the FeFET neurons that are ideal for neuromorphic computing.**

***Index Terms*— Ferroelectric FET, neuromorphic, firing pattern, biomimetic circuits.**

I. Introduction

NEURAL network architectures are experiencing a renaissance because of the recent advances in deep learning models in the field of machine learning and computer vision [1]. Bio-mimetic Spiking Neural Networks (SNN) are receiving traction with applications in visual recognition [2], natural language processing [3] solving constraint satisfaction problems [4]. Further, recent advances of emerging nano-electronic devices and materials such as resistive RAMs [5], spintronics [6] and metal-insulator transition devices [7], are enabling real-time, energy-efficient and large-scale mixed-signal neuromorphic computing hardware [8].

By leveraging the unique characteristics of post-CMOS technologies, researchers have demonstrated electronic neurons with excellent performance, power-efficiency and density. Recently, FeFET based oscillators [9] and spiking neurons with excitatory and inhibitory inputs were proposed [10]. It utilizes the hysteresis of the FeFET and a traditional MOSFET as a switch to charge and discharge a load capacitor, resulting in a periodic generation of voltage spikes (Fig 1). Besides its low-power and 2T compact design, another advantage of this neuron model lies in its adaptive frequency of spikes – a feature which can been empirically noticed in cortical neurons. The two gate voltages imitate the excitatory and inhibitory synaptic inputs of biological neuron, and thus enable various neuromorphic dynamic behavior. Besides [9], [10], FeFET based coupled oscillators [11] have also been proposed. For modeling FeFETs, there are several previous articles that propose physics-based device models by solving the time-dependent Landau-Khalatnikov equation [12]–[16]. Nonetheless, these models are highly compute-intensive, and they remain impractical to simulate neuromorphic systems that consist of large number of coupled FeFET neurons. Further, the FeFET models capture the dynamics of the FeFET only and dynamical models of the spiking neuron circuit are needed.

In our work, we propose a compact dynamical model of the FeFET based spiking neuron. Our physics-driven model focuses on capturing the critical voltages and currents that enable spike timing (phase) and spiking frequency. We demonstrate how such a FeFET neuron faithfully mimics multiple firing patterns of cortical neurons.

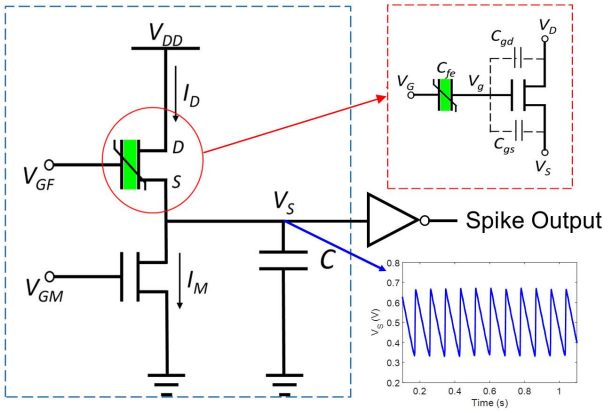

Fig. 1. Schematic of FeFET based spiking neuron. Spikes are generated by a FeFET based relaxation oscillator (blue box) and output through an inverter. The FeFET (red box) is composed of a ferroelectric layer that connected to a common FET. The waveform shows experimental demonstration of the bursting mode for a neuron [10].

II. A Neuron as a Dynamical System

Fig. 1 illustrates the circuit of the FeFET based spiking neuron [10]. Fundamentally, it functions as a relaxation oscillator that periodically charges and discharges capacitor C with I_D and I_M, which are the currents flowing through the two transistors. The pull-up FeFET which charges C, can be viewed as a ferroelectric layer connected to the gate of a normal N-type FET. A traditional pull-down MOSFET is connected to the capacitor and provides a discharging path.

Manuscript received April 17, 2019; revised May 1, 2019; accepted May 1, 2019. Date of publication May 6, 2019; date of current version June 26, 2019. This work was supported by the Semiconductor Research Corporation (SRC) and DARPA. The review of this letter was arranged by Editor A. Chin. *(Corresponding author: Yan Fang.)*

Y. Fang, Z. Wang, A. I. Khan, and A. Raychowdhury are with the School of Electrical and Computer Engineering, Georgia Institute of Technology, Atlanta, GA 30332 USA (e-mail: yan.fang@gatech.edu).

J. Gomez and S. Datta are with the Department of Electrical Engineering, University of Notre Dame, Notre Dame, IN 46556 USA.

Color versions of one or more of the figures in this letter are available online at http://ieeexplore.ieee.org.

Digital Object Identifier 10.1109/LED.2019.2914882

To understand the source of oscillation, let us assume the gate voltages V_{GF}, V_{GM} and V_{DD} are fixed. During the charging phase, the voltage of capacitor C, V_S, is relatively low and triggers the coercion of the ferroelectric layer, injects charge into the gate node V_g and abruptly switches the FeFET to an ON state. Consequently, I_D charges the capacitor throughout this phase. As V_S rises to a certain threshold that initiates the discharging phase, the ferroelectric layer reaches another coercive voltage, removes the charge from V_g and switches the FeFET to an OFF state. Since I_D is now almost zero, I_M is able to discharge the capacitor and V_S decreases. Then the whole process resumes and the two phases are repeated alternatively and V_S keeps oscillating between the two boundary voltages V_{t1} and V_{t2}. For example, Fig 1 illustrates the waveform of V_S, obtained from experimental data in [10] and illustrates the bursting mode of a spiking neuron.

Considering that the switching time of FeFET is very short compared to the oscillation period, we approximate the FeFET as a simple switch in our model. V_{t1} and V_{t2} can be determined by the characteristics of the FeFET and terminal voltages V_G and V_D (V_{GF} and V_{DD}). To locate these two critical voltages, we need to focus on the boundary conditions in terms of charge at the two critical points where the device switches. Thus, we have:

$$\begin{aligned} V_g C_T &= Q_{fe} + C_{fe} V_{GF} + C_{gd} V_{DD} + C_{gs} V_S \\ C_T &= C_{fe} + C_{gd} + C_{gs} \end{aligned} \tag{1}$$

Here we follow the notation of [10], C_{fe} is a linear constant capacitor and Q_{fe} is the bond charge released when the FeFET switches. C_T is the total capacitance at the gate. Here $V_g = V_{GF} - V_{fe}$. V_{fe} is the voltage cross the ferroelectric layer and equals to one of the two coercive voltages, V_{c1} and V_{c2}. From (1) we can obtain the switching boundary voltages, V_{t1} and V_{t2} as:

$$\begin{aligned} V_{ti} &= \alpha^{(i)} - \gamma^{(i)} V_{DD} + \left(1 + \gamma^{(i)}\right)(V_{GF} - V_{ci}), \quad i = 1, 2 \\ \gamma^{(i)} &= \frac{C_{gd}^{(i)}}{C_{gs}^{(i)}}, \quad \alpha^{(i)} = -\left(\frac{C_T V_c^{(i)} + \beta^{(i)} Q_{fe}}{C_{gs}^{(i)}}\right), \quad \beta^{(1,2)} = \pm 1 \end{aligned} \tag{2}$$

$i = 1, 2$ represent the two critical points. $\alpha^{(i)}$, $\gamma^{(i)}$, V_{c1} and V_{c2} are device parameters that can be calibrated through experimental demonstrations [10] or physics-based models. Thus, we can calculate V_{t1} and V_{t2} in terms of V_{GF} and V_{DD}. In the next step, we describe the simplified dynamical behavior of the neuron circuit using a first-order differential equation for V_S:

$$\begin{aligned} \frac{dV_S}{dt} &= \frac{1}{C}(I_D - I_M) \\ I_D &= s g_F (V_g - V_S - V_{Gth}), \quad \begin{cases} s = 0, & V_{t1} \rightarrow V_{t2} \\ s = 1, & V_{t1} \leftarrow V_{t2} \end{cases} \\ I_M &= g_M (V_{GM} - V_{Mth}) \end{aligned} \tag{3}$$

The binary flag $s = 1$ and $s = 0$ represent charging and discharging phases respectively. I_D and I_M are described by simple piecewise linear functions. V_g can be obtained from equation (1). g_F, g_M, V_{Gth} and V_{Mth} are transconductance and threshold voltages of the transistors.

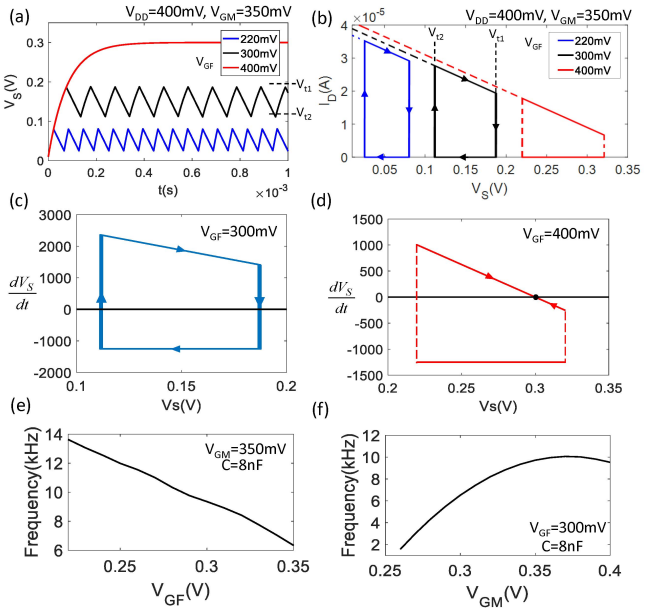

Fig. 2. Demonstration of model simulation: (a) waveforms of V_S (V_{GF} = 220mV, 300mV, and 400mV); (b) I_D - V_S curves of hysteresis loops in (a); (c) (d) flow diagrams of equation (3) (V_{GF} = 300mV, 400mV); (e) V_{GF} v.s. frequency as V_{GM} = 350mV; (f) V_{GM} v.s. frequency as V_{GF} = 300mV.

To verify our model, we apply it to the FeFET oscillator circuit provided in [9] and reproduce the dynamic behavior. In this case, the FeFET is composed of a 10nm HfO_2 ferroelectric layer at the 14 nm FinFET node for which the compact model is described in [17]. The discharging transistor is a FinFET with the same configuration but no ferroelectric layer. We use the same parameters in [9]. V_{DD} is set to 400mV and V_{GM} has a default value of 350mV. C is set to 8nF.

Fig. 2(a) shows the waveforms of V_S from the results of model simulation when different values of V_{GF} are applied (220mV, 300mV, and 400mV). Fig. 2(b) demonstrates the $I_D - V_S$ curves corresponding to each case, showing the FeFET's hysteretic behavior. It is observed that an increase of V_{GF} results in an increase in the hysteresis width $V_{t1} - V_{t2}$ and shifts the hysteresis region of V_S to a higher voltage. This phenomenon is consistent with the observation in [9] and can be explained by equation (2) of the proposed model. It is worth noting that when $V_{GF} = 400$mV, V_S operates in such a high voltage range that the charging and discharge currents balance each other, thus eliminating any oscillation. For better illustration, we plot the flow behavior of the dynamical system from equation (3) in Fig. 2(c) and (d), where the y-axis indicates the derivative of V_S. When $V_{GF} = 300$mV, the line of $dV_S/dt = 0$ crosses the steep transition of the hysteresis. Consequently, the system has no attractor or fixed point and produces spontaneous oscillations. However, when $V_{GF} = 400$mV, $dV_S/dt = 0$ crosses the upper branch of the flow (charging phase) and creates a fixed point near $V_S = 300$mV. The existence of a fixed point attracts V_S to this stable state and eliminates any oscillatory behavior.

If we view the V_S in the non-oscillatory state as being in the resting state of an electronic neuron, the FeFET relaxation oscillator exhibits the same dynamics as a leaky

integrate-and-fire (LIF) spiking neuron, that fires with a reverse polarity, and V_S represents the equivalent of the membrane voltage. In other words, this FeFET neuron fires when V_S reaches a lower threshold voltage, V_{t2} and the spikes are created from V_{DD} to 0. Such dynamical behavior is validated in [10].

Fig. 2(e) and (f) illustrate how V_{GF} and V_{GM} can be used to control the oscillating frequency when one of these two gate voltages is fixed. The frequency shown here is measured as the instantaneous firing rate of spikes, instead of the mean frequency in the power spectrum. From these two diagrams, we notice that increasing V_{GF} decreases the firing rate and can even push the system to a resting state, thus exhibiting a prototypical "inhibitory" behavior. On the other hand, a higher V_{GM} increases the firing rate though faster discharging, and the corresponding input behaves as a prototypical "excitatory" input.

III. Biomimetic Spiking Patterns

It is widely acknowledged that although the standard LIF model is computationally powerful, it cannot mimic the complex dynamics of cortical neurons. The LIF model is one dimensional and cannot faithfully represent the dynamics of multiple channels in biological neurons. Izhikevich proposed an efficient two-dimensional model that mimics most known dynamics in cortical neurons [18]. The key idea is to add one slow variable to tune the leaky current of a LIF model. Inspired from Izhikevich's model, we propose that specific signals can enable the inhibitory input V_{GF} to function as the "slow variable" of the leakage term because the FeFET controls the "discharging" phase of the spike. Combining with the frequency adaption performed by V_{GM}, our model can be used to mimic different types of neuronal dynamics that cannot be achieved by a standard LIF model only.

Fig 3 demonstrates several classes of the spiking dynamics [18] obtained by application of various patterns of V_{GF} and V_{GM}.

- Fast Spiking (FS) and Low Threshold Spiking (LTS): two firing patterns of inhibitory cortical cells. Both of them generate high-frequency spike trains but the latter one has a noticeable spike frequency adaptation
- Regular Spiking (RS) and Thalamo-cortical (TC): regular low-frequency firing patterns from cortical neurons
- Intrinsically Bursting (IB): a stereotypical burst of spikes followed by repetitive single spikes
- Chattering (CH): several stereotypical bursts of closely spaced spikes.

For FS and LTS, the FeFET neuron operates in normal oscillation mode without inhibition (low V_{GF}) to ensure a high firing rate, while V_{GM} can provide frequency adaption of LTS. The single spikes in RS, CT and IB are generated through periodic inhibition with large duty cycles. The short bursts in IB and CH happen when the inhibition signal is OFF and the FeFET neuron returns to an oscillatory mode. This is illustrated in Fig. 3 where the four neuronal dynamics and the corresponding input pulse patterns have been shown. Note that in [10], the spikes outputs are collected after an inverter and the input terminals have RC integrators to accept spike trains from pre-synaptic neurons. In such a design, the neuronal dynamics we discussed above, can be easily achieved with

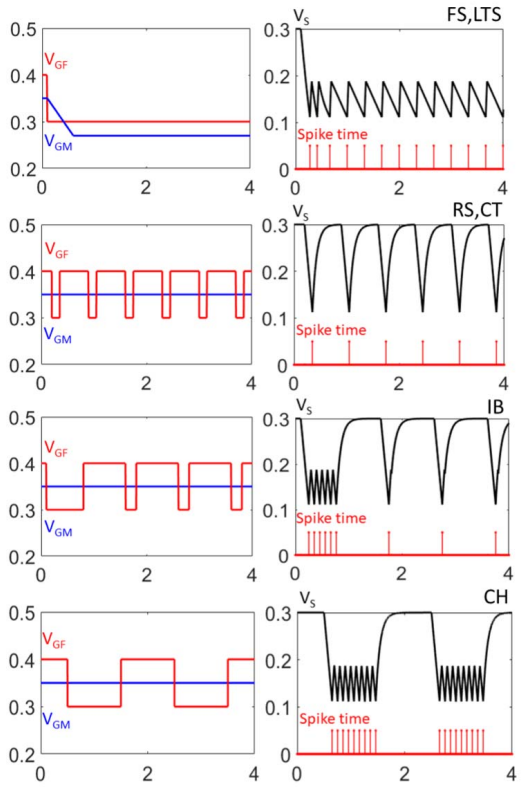

Fig. 3. Spiking patterns of cortical neuron. The left column plots the waveforms of input signals to V_{GF} (red) and V_{GM} (blue). The diagrams on the right column show the waveforms of V_S (black) and corresponding spike timing (red). X-axis: voltage in V. Y-axis: time in ms.

appropriate spiking input signals. Further, the spiking patterns are not limited to the examples mentioned above and other spiking patterns are also possible.

It worth noting that the spike timing and frequency depend on the intrinsic characteristics of FeFET and are affected by the manufacturing variability and cycle-to-cycle variations of the devices. To be specific, the spike time is determined by two factors. One is the critical voltages V_{c1} and V_{c2}, which depend on C_{fe}, C_T and Q_{fe}, according to equation (2). Another factor is the speed of charging, determined by the I_D, which is also impacted by the device variability. However, from the perspective of neuromorphic computing, the variability of FeFET characteristics could be potentially harnessed. Most spiking neural networks require variation for its asymmetric initialization, dynamical bifurcation and stochastic properties in computing. For example, a stochastic winner-takes-all network require each neuron to be asymmetric and stochastic [4].

IV. Conclusion

In this letter, we propose a compact dynamical model of a FeFET based spiking neuron. The proposed model captures the dynamical behavior of the FeFET neuron and models both the spike timing and spiking frequency. We use our model to explain the mechanism of inhibitory input from the FeFET gate and relate it to the computational biological neuron model. Finally, we demonstrate that the FeFET based spiking neuron with different excitatory and inhibitory inputs can imitate various spiking patterns of cortical neurons, similar to the Izhikevich's model of cortical neurons.

REFERENCES

[1] Y. LeCun, Y. Bengio, and G. Hinton, "Deep learning," *Nature*, vol. 521, pp. 436–444, May 2015. doi: 10.1038/nature14539.

[2] Y. Cao, Y. Chen, and D. Khosla, "Spiking deep convolutional neural networks for energy-efficient object recognition," *Int. J. Comput. Vis.*, vol. 113, no. 1, pp. 54–66, 2015. doi: 10.1007/s11263-014-0788-3.

[3] P. U. Diehl, G. Zarrella, A. Cassidy, B. U. Pedroni, and E. Neftci, "Conversion of artificial recurrent neural networks to spiking neural networks for low-power neuromorphic hardware," in *Proc. IEEE Int. Conf. Rebooting Comput. (ICRC)*, Oct. 2016, pp. 1–8. doi: 10.1109/ICRC.2016.7738691.

[4] Z. Jonke, S. Habenschuss, and W. Maass, "Solving constraint satisfaction problems with networks of spiking neurons," *Frontiers Neurosci.*, vol. 10, p. 118, Mar. 2016. doi: 10.3389/fnins.2016.00118.

[5] G. Indiveri, B. Linares-Barranco, R. Legenstein, G. Deligeorgis, and T. Prodromakis, "Integration of nanoscale memristor synapses in neuromorphic computing architectures," *Nanotechnology*, vol. 24, no. 38, p. 384010, Sep. 2013. doi: 10.1088/0957-4484/24/38/384010.

[6] P. A. Merolla, J. V. Arthur, R. Alvarez-Icaza, A. S. Cassid, J. Sawada, F. Akopyan, B. L. Jackson, N. Imam, C. Guo, Y. Nakamura, and B. Brezzo, "A million spiking-neuron integrated circuit with a scalable communication network and interface," *Science*, vol. 345, no. 6197, pp. 668–673, Aug. 2014. doi: 10.1126/science.1254642.

[7] A. Parihar, M. Jerry, S. Datta, and A. Raychowdhury, "Stochastic IMT (insulator-metal-transition) neurons: An interplay of thermal and threshold noise at bifurcation," *Front. Neurosci.*, vol. 12, p. 210, Apr. 2018. doi: 10.3389/fnins.2018.00210.

[8] M. Romera, P. Talatchian, S. Tsunegi, F. A. Araujo, V. Cros, P. Bortolotti, J. Trastoy, K. Yakushiji, A. Fukushima, H. Kubota, S. Yuasa, M. Ernoult, D. Vodenicarevic, T. Hirtzlin, N. Locatelli, D. Querlioz, and J. Grollier, "Vowel recognition with four coupled spin-torque nano-oscillators," *Nature.*, vol. 563, no. 7730, pp. 230–234, Oct. 2018. doi: 10.1038/s41586-018-0632-y.

[9] Z. Wang, S. Khandelwal, and A. I. Khan, "Ferroelectric oscillators and their coupled networks," *IEEE Electron Device Lett.*, vol. 38, no. 11, pp. 1614–1617, Nov. 2017. doi: 10.1109/LED.2017.2754138.

[10] Z. Wang, B. Crafton, J. Gomez, R. Xu, A. Luo, Z. Krivokapic, L. Martin, S. Datta, A. Raychowdhury, and A. I. Khan, "Experimental demonstration of ferroelectric spiking neurons for unsupervised clustering," in *IEDM Tech. Dig.*, Dec. 2018, pp. 13.3.1–13.3.4. doi: 10.1109/IEDM.2018.8614586.

[11] N. Thakuria, A. K. Saha, S. K. Thirumala, B. Jung, and S. K. Gupta, "Oscillators utilizing ferroelectric-based transistors and their coupled dynamics," *IEEE Trans. Electron. Devices.*, vol. 66, no. 5, pp. 2415–2423, May 2019. doi: 10.1109/TED.2019.2902107.

[12] A. I. Khan, C. W. Yeung, C. Hu, and S. Salahuddin, "Ferroelectric negative capacitance MOSFET: Capacitance tuning & antiferroelectric operation," in *IEDM Tech. Dig.*, Dec. 2011, pp. 11.3.1–11.3.4.

[13] A. Aziz, S. Ghosh, S. Dutta, and S. K. Gupta, "Physics-based circuit-compatible SPICE model for ferroelectric transistors," *IEEE Electron Device Lett.*, vol. 37, no. 6, pp. 805–808, Jun. 2016. doi: 10.1109/LED.2016.2558149.

[14] P. Lenarczyk and M. Luisier, "Physical modeling of ferroelectric field-effect transistors in the negative capacitance regime," in *Proc. Int. Conf. Simulation Semiconductor Process. Devices (SISPAD)*, Sep. 2016, pp. 311–314. doi: 10.1109/SISPAD.2016.7605209.

[15] A. Aziz, E. T. Breyer, A. Chen, X. Chen, S. Datta, S. K. Gupta, M. Hoffmann, X. S. Hu, A. Ionescu, M. Jerry, T. Mikolajick, H. Mulaosmanovic, K. Ni, M. Niemier, I. O'Connor, A. Saha, S. Slesazeck, S. K. Thirumala, and X. Yin, "Computing with ferroelectric FETs: Devices, models, systems, and applications," in *Proc. Design, Automat. Test Eur. Conf. Exhib. (DATE)*, Mar. 2018, pp. 1289–1298. doi: 10.23919/DATE.2018.8342213.

[16] A. Dasgupta, P. Rastogi, D. Saha, A. Gaidhane, A. Agarwal, and Y. S. Chauhan, "Modeling of multi-domain switching in ferroelectric materials: application to negative capacitance FETs," in *IEDM Tech. Dig.*, Dec. 2018, pp. 9.2.1–9.2.4. doi: 10.1109/IEDM.2018.8614539.

[17] S. Khandelwal, J. P. Duarte, A. I. Khan, S. Salahuddin, and C. Hu, "Impact of parasitic capacitance and ferroelectric parameters on negativecapacitance FinFET characteristics," *IEEE Electron Device Lett.*, vol. 38, no. 1, pp. 142–144, Jan. 2017. doi: 10.1109/LED.2016.2628349.

[18] E. M. Izhikevich, "Simple model of spiking neurons," *IEEE Trans. Neural Netw.*, vol. 14, no. 6, pp. 1569–1572, Nov. 2003. doi: 10.1109/TNN.2003.820440.